Structural Stability of Carbon Nanotube Films: The Role of Bending Buckling

Alexey N. Volkov and Leonid V. Zhigilei*

Department of Materials Science and Engineering, University of Virginia, 395 McCormick Road, Charlottesville, Virginia 22904-4745, United States

ARTICLE

ABSTRACT In films, mats, buckypaper, and other materials composed of carbon nanotubes (CNTs), individual CNTs are bound together by van der Waals forces and form entangled networks of bundles. Mesoscopic dynamic simulations reproduce the spontaneous self-assembly of CNTs into continuous networks of bundles and reveal that the bending buckling and the length of CNTs are the two main factors responsible for the stability of the network structures formed by defect-free CNTs. Bending buckling of CNTs reduces the bending energy of interconnections between bundles and stabilizes the interconnections by creating effective barriers for CNT sliding. The length of the nanotubes is affecting the ability of van der Waals forces of intertube interactions to counterbalance the internal straightening forces acting on curved nanotubes present in the continuous networks. The critical length for the formation of stable network structures is found to be ~120 nm for (10,10) single-walled CNTs. In the simulations where the bending buckling is artificially switched off, the network structures are found to be unstable against disintegration into individual bundles even for micrometer-long CNTs.

KEYWORDS: carbon nanotube materials · buckypaper · mesoscopic simulations · bending buckling · stability of network materials

The network materials composed of carbon nanotubes (CNTs) are attracting an increasing attention due to the diverse range of their potential applications, from making flexible/stretchable electronic and acoustic devices[1,2] to fabrication of nanocomposite materials with improved fire retardancy[3] and mechanical properties.[4,5] In these materials, commonly referred to as CNT films, mats, or buckypaper, the van der Waals interactions among nanotubes result in their agglomeration into close-packed bundles[6,7] which, in turn, form continuous entangled network structures.[4,5,7−11] The microscopy images taken from the CNT films produced by different methods are surprisingly similar in their visual appearance, suggesting the presence of mechanisms that stabilize the network structures and limit coarsening of the CNT bundles. Indeed, while quantitative structural parameters of CNT films and mats exhibit some dependence on the material synthesis procedures, the bundle diameters in CNT materials synthesized by different methods are typically limited to several tens of nanometers,[4−6,11] with corresponding numbers of individual CNTs in a bundle ranging from several to a few hundred of CNTs.[6] In the absence of chemical cross-links between the CNTs, the tensile strength of the CNT films is relatively low, typically in the range from 5 to 30 MPa.[9−12] Nevertheless, the CNT materials exhibit sufficient mechanical stability to be handled in the form of free-standing thin films.[1,2,4,5,8,11,12]

Despite the growing number of practical applications and experimental investigations, the theoretical/computational studies of CNT materials have been scarce. The complex mesoscopic structural organization of the continuous networks of bundles hampers application of well-established atomistic or continuum models. As a result, the computational efforts in this area have been limited to application of simplified models based on consideration of random contacts in a system of fibers representing bundles of nanotubes[10,13,14] or analysis of CNT arrangements in bundles or forests of vertically aligned nanotubes.[15−18] Recent development of a mesoscopic model capable of a computationally efficient dynamic simulation of systems consisting of a large number of interacting nanotubes[19,20] enabled first simulations of self-organization of nanotubes into random networks of bundles[20,21] and opened a new opportunity for a more realistic computational treatment of CNT materials.[22] In this paper we report the results of a computational investigation of the factors responsible for self-organization of CNTs into mechanically stabile and reproducible network structures characteristic of CNT films and mats. Along with the length of CNTs, the

*Address correspondence to lz2n@virginia.edu.

Received for review July 9, 2010 and accepted September 28, 2010.

Published online October 8, 2010.
10.1021/nn1015902

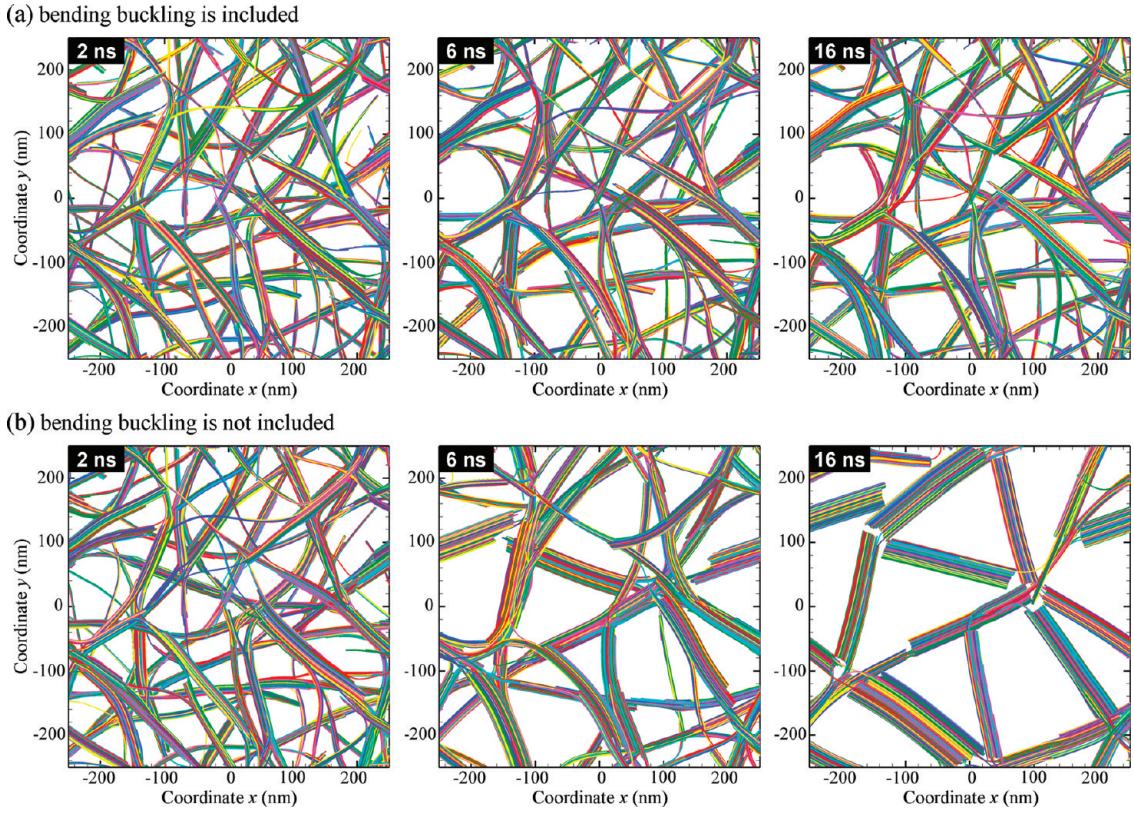

Figure 1. Evolution of the structure of nanotube networks in the course of simulations performed at a temperature of 300 K for a 20 nm film composed of (10,10) CNTs. The number of CNTs in the computational system is 1543, the length of each CNT is 200 nm, and the density of the film is 0.2 g cm^{-3}. Bending buckling is accounted for in the simulation shown in (a) and is not taken into account in the simulation shown in (b). The initial structure at the beginning of the simulations (at 1 ns) is identical in both simulations. Different nanotubes are colored by different (random) color in the snapshots.

bending buckling of individual nanotubes forming interconnections between bundles is found to play a critical role in stabilization of well-connected networks of curved CNT bundles.

RESULTS AND DISCUSSION

Using the mesoscopic force field briefly described in the Computational Method Section, we perform a series of dynamic simulations aimed at the investigation of the factors affecting the structural stability of the network structures characteristic of CNT films and mats. The simulations are performed for films consisting of (10,10) single-walled CNTs, with a film thickness ranging from 20 to 200 nm and a density ranging from 0.05 to 0.4 g cm^{-3}. All nanotubes in a given film have the same length L_T, and systems with a L_T from 20 nm to 1 μm are studied. The equilibrium length of segments in the mesoscopic representation of CNTs is chosen to be 2 nm, more than an order of magnitude smaller than the critical radius of curvature for the onset of nanotube bending buckling, R_{cr}. The range of the film thickness and density as well as the values of L_T considered in the simulations are typical for thin CNT films produced in experiments.[1,2,7] The initial samples used in the simulations are generated by stacking thin layers of straight nanotubes with a distance between the layers chosen to ensure interlayer interaction.[23] The periodic boundary conditions are applied in the directions parallel to the film surfaces (along the *x*- and *y*-axes). The film density is maintained constant by two planes enclosing the film from the two sides in the z direction and interacting with CNTs by a short-range repulsive potential, U_E in eq 1.

The dynamic simulations consist of two distinct stages. At the first stage, lasting 1 ns, each system of interacting CNTs is allowed to evolve freely, with forces acting on CNTs defined by the mesoscopic force field given by eq 1. The van der Waals interactions between nanotubes steer the evolution of the systems in the direction of fast self-assembly of the CNTs into bundles.[20,21,23] In systems consisting of sufficiently long CNTs ($L_T \geq 60$ nm), the bundles form a continuous network spanning the entire film, whereas shorter nanotubes ($L_T < 60$ nm) self-organize into separate bundles. For the longer CNTs, the structures of continuous networks of CNT bundles produced at the first stage of the simulations are similar to the structures observed in the experimental images of CNT materials.[4−11] In particular, in a good agreement with experimental

measurements,[5,6,11] the diameters of the majority of CNT bundles in the simulated network structures range from 1 to 30 nm, with a few thicker bundles present in some of the networks. The networks contain multiple interconnections between bundles formed by CNTs that belong to two or more bundles simultaneously. Such interconnections can also be identified in experimental images of ultrathin CNT films, *e.g.*, ref 24.

Note that the spontaneous self-assembly of CNTs into bundles is only possible with a realistic description of van der Waals intertube interactions provided by the tubular potential.[20,21] A recent simulation of large groups of interacting CNTs, represented by a bead-and-spring model,[25] failed to reproduce the formation of the continuous networks of bundles observed in experiments. Although the same method of deposition of layers of CNTs, suggested in ref 23 and used in the present work, is adopted in the mesoscopic simulations reported in ref 25, the interactions between the beads in the coarse-grained model introduce large artificial barriers for long-range rearrangements of CNTs required for self-assembly of CNTs into continuous networks of bundles. As a result, the structures obtained with the bead-and-spring model are closer to the layered systems of randomly oriented individual CNTs that, experimentally, can be produced by a layer-by-layer assembly of chemically functionalized and charged nanotubes[26] or by other methods where modification of CNTs counteracts the intertube van der Waals interactions and prevents self-organization of CNTs into bundles.

The structural stability of the networks of CNT bundles produced at the first constant-energy stage of the simulations is investigated at the second stage, when the simulations are continued for additional 9−15 ns under conditions of constant temperature, maintained at 300 K by scaling the velocities of the nodes representing CNTs in the mesoscopic model (see the Computational Method Section) according to the Berendsen thermostat method.[27] The temperature T is defined as $T = 2Q/3Nk_B$, where Q is the kinetic energy associated with the $3N$ dynamic degrees of freedom of the model, N is the total number of CNT nodes, and k_B is the Boltzmann constant. The equilibrium between the low-frequency vibrational modes associated with the dynamic degrees of freedom and the high-frequency atomic vibrations that are not explicitly represented in the mesoscopic model is assumed in the thermostat simulations.

The evolution of the network structure generated in a film composed of CNTs with a length of 200 nm is illustrated in Figure 1a. The "skeleton" of thick bundles generated by the end of the first nanosecond of the constant-energy simulation remains largely unchanged during the constant-temperature

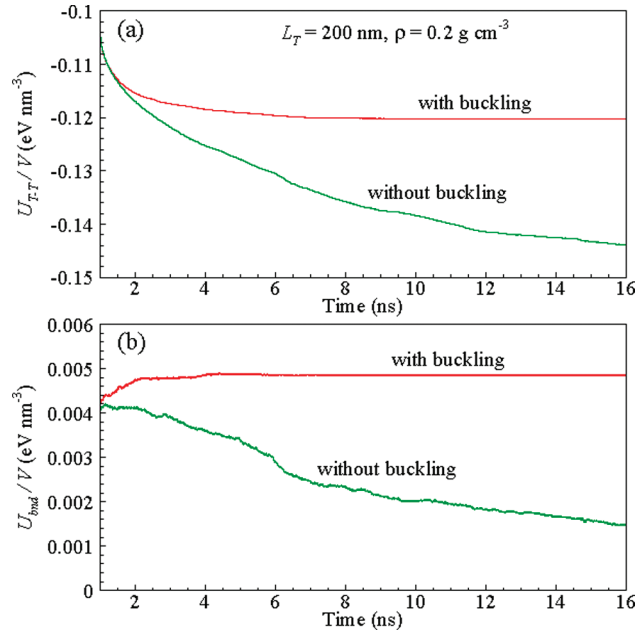

Figure 2. Time dependence of (a) the intertube interaction energy density U_{T-T}/V (V is the total volume of the sample) and (b) the bending energy density U_{bnd}/V in the constant 300 K temperature part of simulations performed for a 20 nm film composed of 200 nm long (10,10) CNTs. The density of the film is 0.2 g cm^{-3}. Results obtained with and without bending buckling included in the mesoscopic force field are shown by red and green curves, respectively. Snapshots from the simulations are shown in Figure 1.

stage of the simulation, with structural changes taking the form of gradual coarsening of the bundles. The coarsening proceeds by thin bundles and remaining individual nanotubes joining the thicker bundles. Within the thick bundles, the nanotubes rearrange to increase the degree of close-packed hexagonal ordering[20] that corresponds to the minimum of the potential energy of the intertube interaction and has been observed in experiments.[6,7] The structural changes in the CNT networks are reflected in a substantial decrease of the intertube interaction energy and a relatively minor increase in the bending energy of the system, as shown by the red curves in Figure 2. The evolution of the structure slows down with time, and the continuous network of CNT bundles formed by the time of ~8 ns appears to be stable against the thermal fluctuations at room temperature. This conclusion can be confirmed by the visual similarity of the structures shown for 6 and 16 ns in Figure 1a as well as by the saturation of the time dependencies of bending and intertube interaction energy densities in Figure 2.

The results of the simulations performed for films of various thickness and density suggest that the observations described above for a 20 nm film with density of 0.2 g cm^{-3} have relatively weak sensitivity to these parameters of the system. In particular, the CNT network structures obtained in simulations performed for L_T = 200 nm and film thicknesses of 100 and 200 nm are found to

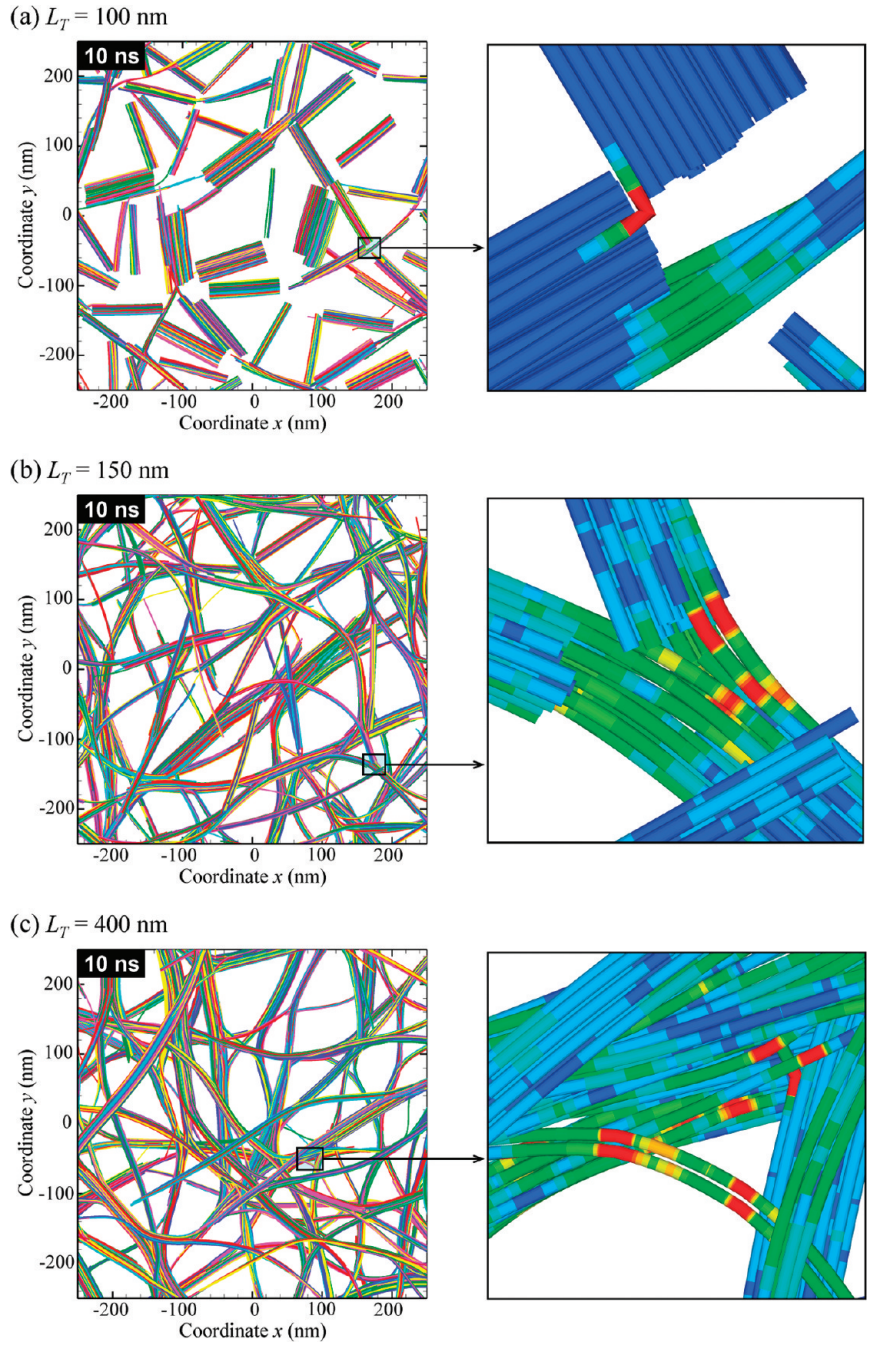

Figure 3. Nanotube networks obtained in simulations performed for 20 nm films composed of (10,10) CNT of different lengths: (a) 100, (b) 150, and (c) 400 nm. Snapshots from the simulations are shown for the same time of 10 ns (1 ns of constant energy simulation followed by 9 ns of constant temperature simulation at 300 K). Mesoscopic force field used in the simulations accounts for the bending buckling of the nanotubes. The density of all films is 0.2 g cm^{-3}. Nanotubes are colored by different (random) color in the left panels. Right panels show enlarged views of structural elements of CNT networks, with nanotube segments colored according to the local radii of curvature. The red color in the right panels marks the segments adjacent to buckling kinks.

be similar to the one shown in Figure 1a for a 20 nm film. The process of CNT self-organization into networks of bundles and structural stability of the networks are also found to be qualitatively similar for films with densities in the range from 0.05 to 0.4 g cm^{-3}, although the structural characteristics of the networks, *e.g.*, size distribution of openings in the porous films and thickness of bundles, are affected by the density.

The length of the CNTs, on the other hand, has a stronger effect on the time scale of the evolution of the network structures and their stability. For short CNTs ($L_T \leq 120$ nm) the network structures generated at the first stage of the simulations are unstable and disintegrate into individual CNT bundles upon relaxation at 300 K. The disintegration proceeds through the formation of intermediate cellular structures composed of

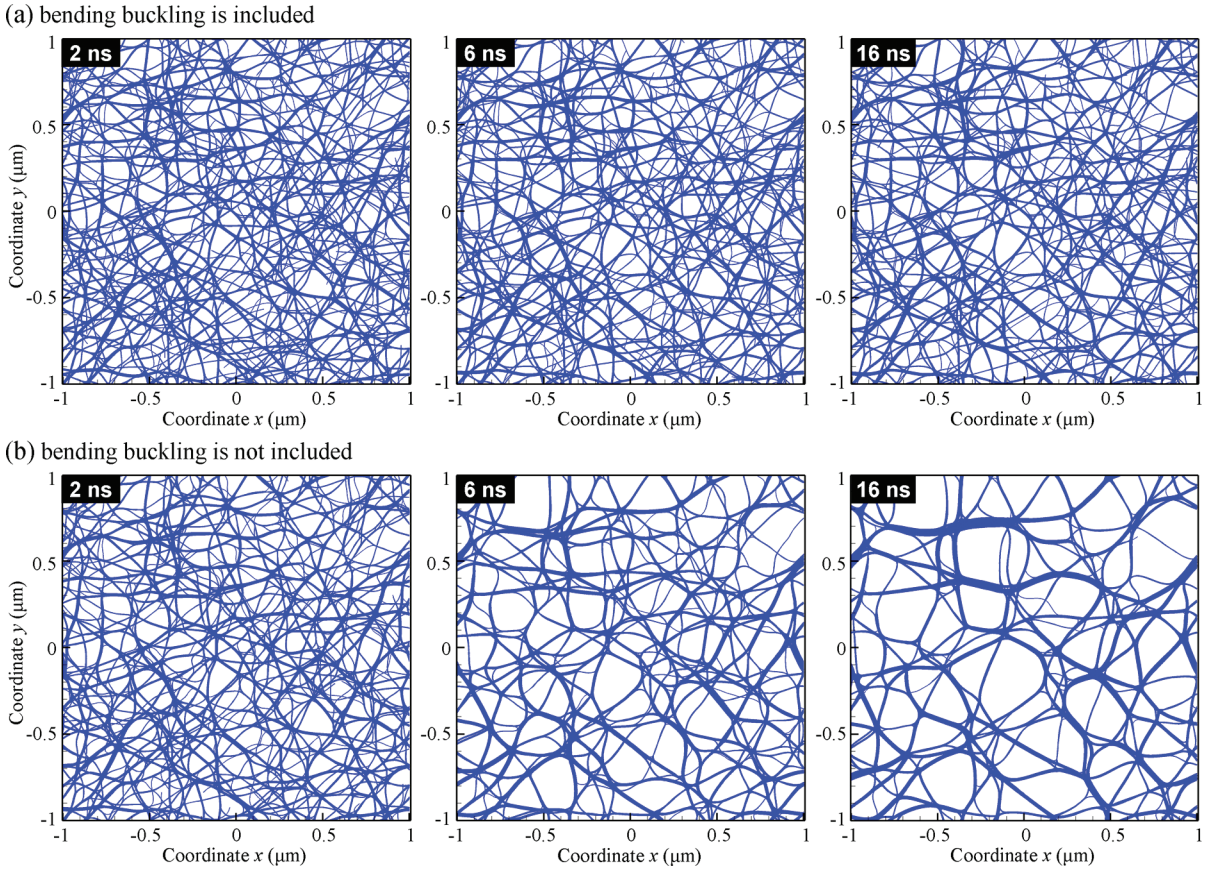

Figure 4. Evolution of the nanotube networks in the course of simulations performed at a temperature of 300 K for a 20 nm film composed of (10,10) CNTs. The number of CNTs in the computational system is 2501, the length of each CNT is 1 μm, and the density of the film is 0.1 g cm^{-3}. Bending buckling is accounted for in the simulation shown in (a) and is not taken into account in the simulation shown in (b).

CNT bundles weakly connected with each other, *e.g.*, Figure 3a for $L_T = 100$ nm. The CNTs in the individual bundles tend to align their ends to further minimize the intertube interaction energy. The network structures composed of longer CNTs remain stable, as shown in Figure 1a for $L_T = 200$ nm and in Figures 3b and 4c for $L_T = 150$ and 400 nm, respectively. The visual difference between the cellular and network structures obtained in the simulations is reflected in quantitative parameters of the structures, such as the bending energy density U_{bnd}/V, where U_{bnd} is the total bending energy of all nanotubes in the sample, and V is the volume of the sample. At a time of 10 ns after the beginning of the simulations, U_{bnd}/V is equal to 0.001 eV nm^{-3} for $L_T = 100$ nm, 0.0057 eV nm^{-3} for $L_T = 150$ nm, 0.0048 eV nm^{-3} for $L_T = 200$ nm, and 0.0068 eV nm^{-3} for $L_T = 400$ nm. The 5-fold raise in the bending energy upon the increase of L_T from 100 to 150 nm signifies the formation of a stable continuous network of CNT bundles.

Detailed analysis of the structures of the CNT networks shows that many of the nanotubes that serve as interconnections between the bundles are buckled. This observation is consistent with the results of TEM imaging[28] of high aspect ratio CNTs, suggesting that bending buckling is a common feature in systems of interacting CNTs. Several examples of the buckling kinks can be seen in enlarged views of typical interconnects shown in Figure 3, where the CNT segments adjacent to the buckling kinks are colored red. The total number of buckling kinks in the network structures is relatively small. For example, in the structure shown in Figure 1a for 16 ps, the total number of kinks is equal to 814. Many of the nanotubes that serve as interconnections between the bundles have multiple kinks, whereas ~70% of the total number of CNTs in this network do not have any buckling kinks. Despite the small number of buckled nanotubes, the bending buckling is found to play a major role in stabilization of the network structures. The connection between the stability of the CNT networks and the bending buckling is 2-fold. First, the transition from quadratic to linear dependence of the bending strain energy on the bending angle (Figure 6b) reduces the energy penalty for the presence of highly bent CNTs at some of the interconnections between the bundles. Second, and more importantly, the buckling kinks play a role of "defects" that impede the relative sliding of nanotubes and, therefore, make the interconnections stable.

The critical role of bending buckling in stabilization of CNT networks becomes apparent from the results of

simulations performed with a mesoscopic force field that does not allow for buckling to occur, *i.e.*, with the bending energy U_{bnd} defined by eq 2 for any local radius of curvature. The results of one of such simulations performed for CNTs with $L_T = 200$ nm are illustrated in Figure 1b. Snapshots from the simulation indicate that the continuous network structure becomes unstable and gradually disintegrates into a cellular structure composed of individual bundles weakly connected with each other. The decomposition of the continuous network of bundles into the cellular structure is driven by the energy minimization. In the absence of the buckling kinks, CNTs that serve as interconnections between bundles are free to slide and join one of the bundles. As the nanotubes gradually slip into the bundles and simultaneously straighten, the energy of intertube interactions and the bending strain energy are both decreasing. Indeed, the energy plots, shown for this simulation by green curves in Figure 2, exhibit a steady decrease of both energy components that do not show any sign of saturation by the end of the simulation. One can expect that the system evolves in the direction of individual bundles of straight CNTs with minimum or no interbundle interaction.

While the decomposition of the continuous network of CNT bundles in the absence of bending buckling slows down with increasing length of CNTs, it cannot be avoided even for micrometer-long CNTs. This is illustrated in Figure 4, where snapshots from two simulations performed for CNTs with $L_T = 1000$ nm are shown. In the simulation performed with bending buckling included in the mesoscopic force field, a stable network structure is generated by the time of ~5 ns, as evidenced by the similarity of snapshots shown for 6 and 16 ns in Figure 4a. Without bending buckling, however, the network structure continues to coarsen, and the energy of the system continues to decrease for the whole duration of the simulation, Figure 4b. Despite the longer time of decomposition of the network structure composed of longer CNTs, one can expect that, similar to the systems of shorter CNTs, the final structure will consist of individual bundles weakly interacting with each other.

Thus, the results of the mesoscopic simulations suggest that the formation of a stable continuous network of CNT bundles is only possible when bending buckling is included in the simulations and when the length of the nanotubes exceeds a certain critical value, found in this work to be ~120 nm for (10,10) single-walled CNTs. The existence of the critical length can be explained by the unavoidable bending of nanotubes included into a continuous network structure. In a stable CNT network, the internal torque acting on an individual bent and buckled CNT acts to straighten the CNT and has to be counterbalanced by a torque originated from intertube van der Waals interactions.[29,30] The maximum bending torque that can be supported by the van der

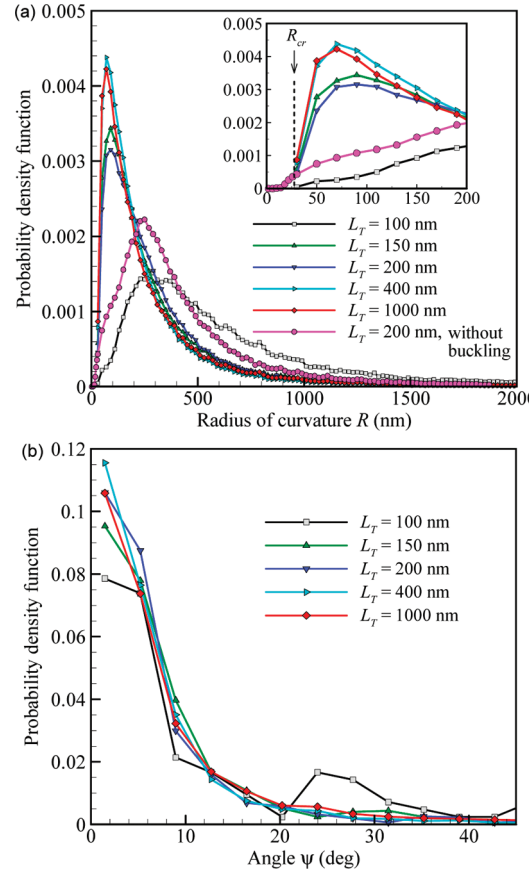

Figure 5. Probability density functions of local radius of CNT curvature R (a) and angle ψ at the buckling kinks (b) in several systems generated in mesoscopic simulations. The results are shown for 20 nm films composed of CNTs with length L_T equal to 100, 150, 200, 400, and 1000 nm. The density of the films is 0.1 g cm^{-3} for $L_T = 1000$ nm and 0.2 g cm^{-3} for all other L_T. The analysis is performed for configurations obtained by the time of 10 ns in the simulations. The probability distribution functions are calculated for simulations with bending buckling accounted for, except for one function shown in (a) for the simulation illustrated in Figure 1b. The inset in (a) shows an enlarged view of the functions at small R. The vertical dashed line in the inset marks the value of the critical curvature R_{cr} for the onset of bending buckling. In (b), ψ = 0 corresponds to the onset of buckling, when the local radius of curvature of a nanotube is equal to R_{cr}.

Waals intertube interactions decreases with decreasing length of the nanotubes. Below a certain critical length, the intertube interaction forces are not sufficiently strong for counterbalancing the internal straightening torques of the bent and buckled nanotubes, and the network disintegrates into a cellular structure composed of individual bundles, *e.g.*, Figure 3a. The critical length of CNTs for the formation of the continuous network of bundles depends on both the bending stiffness of the nanotubes and the parameters of the buckling behavior. To illustrate the latter factor, several additional simulations are performed with the critical radius of curvature, R_{cr}, artificially increased from 27.5 to 41.25 nm, while keeping the bending force constant K_{bnd} and the dimensionless parameter $K_{bcl}R_{cr}/K_{bnd}$ the

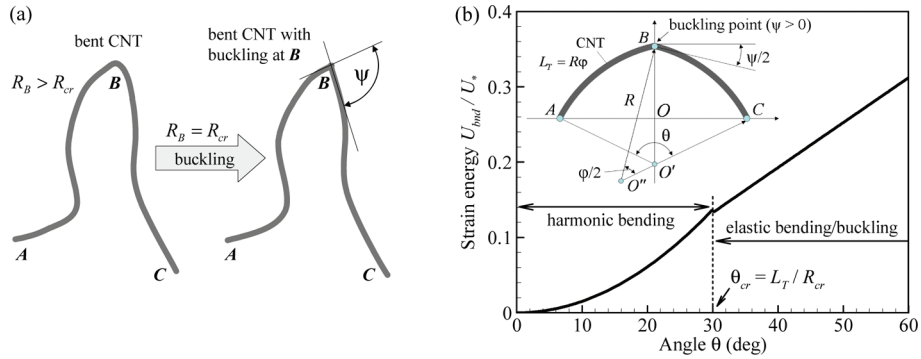

Figure 6. Schematic representation of the description of bending buckling in the mesoscopic model (a) and the dependence of the bending energy U_{bnd} on the bending angle θ in a uniformly bent CNT with a single buckling point appearing in the middle (point B in the inset) when the critical radius of curvature, R_{cr}, is reached (b). Bending energy in (b) is calculated with eq 2 for $\theta < \theta_{cr}$ and is obtained by minimization of the strain energy associated with bending and buckling, $U_{bnd} = K_{bcl}\psi^n + K_{bnd}\varphi^2/(2L_T)$, for $\theta > \theta_{cr}$. Values of the bending energy in (b) are scaled by $U_* = K_{bnd}/L_T$.

same, as in the simulations discussed above. The earlier onset of buckling reduces the bending energy of CNTs and facilitates the formation of stable network structures. In particular, a stable continuous network of bundles was observed in this case in a simulation performed for $L_T = 100$ nm.

The degree of bending deformation of nanotubes included in the network structures can be quantitatively characterized by the probability density function of the local radius of curvature R, $f(R)$. This function is defined so that $L_\Sigma f(R)dR$ is equal to the part of the total length L_Σ of CNTs in the sample where the local radius of curvature is between R and $R + dR$. The results of the calculation of $f(R)$ for several systems are shown in Figure 5a. The distributions calculated for the continuous network structures have the most probable radii of curvature in the range from 50 to 100 nm. The distributions are sharper for films composed of longer nanotubes, with both the most probable and mean radii of curvature decreasing with an increase in CNT length. This observation is consistent with the above discussion of the role of the van der Waals intertube interactions in counterbalancing the internal forces associated with bending strain of the CNTs. The longer the parts of the CNTs that are incorporated into the bundles, the larger is the bending deformation that can be maintained in the network structure. The probability density functions are also calculated for two systems where the network structures have decomposed into the cellular structures consisting of visually straight bundles, a system with $L_T = 100$ nm and a system with $L_T = 200$ nm with no buckling allowed. In these cases, the most probable radius of curvature increases to ~260 nm, and the distributions reveal a large fraction of CNT segments with local radii of curvature that are much larger than the length of the CNTs. This high radius of curvature tail of the distributions is growing with time and reflects the increase in the total length of well-aligned (almost parallel) parts of the CNTs in the visually straight CNT bundles (Figures 1b and 3a).

The distribution of angle ψ at the buckling kinks shown in Figure 5b indicates that, despite the transition from quadratic to linear dependence of the bending strain energy on the bending angle upon buckling, most of the kinks are characterized by $\psi \leq 20°$, suggesting a relatively moderate effect of buckling on the overall shapes of the CNTs, *e.g.*, Figure 3b and 3c. In the simulation where the network of short CNTs decomposes into a cellular structure, however, a substantial number of buckling kinks with large angles ($\psi > 20°$), Figure 6, appears in the remaining CNTs connecting the bundles, *e.g.*, Figure 3a.

CONCLUSIONS

The mesoscopic simulations of systems composed of a large number of interacting CNTs predict spontaneous self-assembly of CNTs into continuous networks of bundles with partial hexagonal ordering of CNTs within the bundles. Detailed analysis of the computational results reveals the dominant role of the bending buckling in the generation and stabilization of the network structures. The buckling not only reduces the bending energy of curved CNTs that make up the interconnections between the bundles but also stabilizes the interconnections by creating effective barriers for CNT sliding. For (10,10) single-walled CNTs, the formation of stable continuous networks of bundles is observed in all simulations performed for CNTs that are longer than ~120 nm. If, however, the buckling behavior is not included in the model, the continuous networks of bundles disintegrate into cellular structures consisting of individual bundles weakly connected with each other. There are a number of additional factors that may contribute to the stabilization of the network structures in real materials composed of CNTs with various structural defects. The generation of covalent bonds between CNTs,[13,31] the static friction between CNTs associated with structural defects and/or presence of amorphous carbon,[32,33] as well as the presence of intrinsic kinks in as-grown

CNTs[34] could serve as additional barriers for decomposition and coarsening of the network structures. The simulations reported in this paper, however, suggest that the formation of the buckling kinks alone is capable of stabilizing the continuous networks composed of perfect defect-free CNTs.

COMPUTATIONAL METHOD

Mesoscopic Dynamic Model for CNT Materials. The continuous network structures of CNT bundles are generated in simulations performed with a mesoscopic dynamic model that represents individual CNTs as chains of stretchable cylindrical segments.[19] The CNTs are defined by positions of nodes jointing the neighboring segments, and the dynamics of a system of interacting CNTs is described by solving the equations of motion of classical mechanics for the positions of all nodes. The forces acting on the nodes are calculated based on the mesoscopic force field that accounts for stretching and bending deformations of individual CNTs[19] as well as for the van der Waals interactions among the CNTs.[20] The potential energy of the system can be written as

$$U = U_{str} + U_{bnd} + U_{T-T} + U_E \quad (1)$$

where U_{str} and U_{bnd} correspond to the strain energy associated with stretching and bending of individual CNTs, U_{T-T} is the energy of intertube interactions, and U_E is the energy of interaction between nanotubes and external bodies. The latter term is used in this work to confine CNT films between two planes and to ensure constant density conditions in the dynamic simulations. A description of forces related to intertube friction is not included in the mesoscopic force field as these forces are too weak to prevent room-temperature rearrangements of defect-free CNTs.[32,33] In particular, the values of static friction forces recently measured for pairs of annealed nearly perfect CNTs are found to be independent of the overlap area and are consistent with theoretical estimations of forces related to van der Waals intertube interactions.[34] These forces, originating from the changes in the intertube interaction area, are naturally accounted for in the mesoscopic model.

The harmonic parts of the stretching and bending potentials, U_{str} and U_{bnd}, are parametrized for single-walled CNTs in ref 19 based on the results of atomistic simulations performed with the reactive empirical bond-order (REBO) potential.[35,36] The transition to the anharmonic regime (nonlinear stress−strain dependence) and a description of fracture of CNTs under tension are included in U_{str} but do not play a role under conditions of the simulations performed in this study. The axial buckling of CNTs under uniaxial compression is not accounted for in the current version of the model since the compressive strains in the simulations are far below the critical axial buckling strain of ~5% for (10,10) CNTs.[37] The bending buckling, on the other hand, is found to play a critical role in stabilization of the continuous network structures of CNT bundles, and the description of the bending buckling in the mesoscopic model is provided below. The intertube interaction term U_{T-T} is calculated based on the tubular potential method[20,21] that allows for a computationally efficient and accurate representation of van der Waals interactions between CNT segments of arbitrary lengths and orientation. The tubular potential is parametrized based on an interatomic potential for nonbonded interactions between carbon atoms adopted from the adaptive intermolecular REBO (AIREBO) potential[38] and is found to reproduce the predictions of the atomistic representation of the intertube interactions (summation over pairs of interacting atoms) with high accuracy at a tiny fraction of the computational cost.[20]

Mesoscopic Description of Bending Buckling. The mesoscopic description of bending buckling is based on the results of atomistic[39−45] and continuum[42,44,45] simulations that consistently predict a quadratic dependence of the strain energy of a bent nanotube on the bending angle θ in the prebuckling state and an approximately linear dependence on θ in the postbuckling state. In the prebuckling state, the bending energy term for a single nanotube can be written as

$$U_{bnd} = \int_A^C \frac{1}{2}\frac{K_{bnd}}{R^2} dl \quad (2)$$

where R is the local radius of curvature of the elastic line of the nanotube, K_{bnd} is the bending force constant, and the integration is performed along the length l of the elastic line (Figure 6a). For a uniformly bent nanotube of length L_T, the bending angle θ is related to the radius of curvature R as $\theta = L_T/R$, and eq 2 reduces to $U_{bnd} = K_{bnd}\theta^2/(2L_T)$, *i.e.*, the model corresponds to the harmonic potential with respect to the bending angle.

For the bending energy of a buckled nanotube, the predictions of atomistic simulations can be well reproduced by the following formulation of the bending energy term:

$$U_{bnd} = K_{bcl}\psi^n + \int_A^B \frac{1}{2}\frac{K_{bnd}}{R^2} dl + \int_B^C \frac{1}{2}\frac{K_{bnd}}{R^2} dl \quad (3)$$

where $K_{bcl}\psi^n$ is the term representing the energy of the buckling kink in the mesoscopic model, and ψ is the angle between two tangents to the elastic line at the point of kink (point B in Figure 6a). The transition from eqs 2 to 3 in the description of the bending energy takes place when the local radius of curvature R drops down to the critical curvature for the onset of buckling, R_{cr}, *e.g.*, when $R_B = R_{cr}$ in Figure 6a. To ensure that U_{bnd} is approximately proportional to θ in the postbuckling state,[39−41,43−45] the value of n is set to unity. The remaining parameters of the bending energy term depend on the radius and chirality of CNTs and can be chosen based on the results of atomistic simulations performed for uniformly bent CNTs with a single buckling kink, as shown in Figure 6b. For (10,10) single-walled CNTs, $K_{bnd} = 1.9 \times 10^4$ eV Å is chosen to match the results of the simulations performed with the REBO potential,[19] $R_{cr} = 27.5$ nm is selected to be within the range from 23.5 to 31.3 nm predicted in refs 42, 43, and 45, and K_{bcl} is obtained from the approximate equation $K_{bcl}R_{cr}/K_{bnd} = 0.7$ that brings the ratio of slopes $dU_{bnd}/d\theta$ in the pre- and postbuckling states at $R = R_{cr}$ into a good quantitative agreement with the results of atomistic simulations performed for various single-walled CNTs.[39−41,43−45]

Acknowledgment. Financial support for this work was provided by NSF (award CBET-1033919) and NASA (award NNX07AC41A). Computational support was provided by NCCS at ORNL (project no. MAT009).

REFERENCES AND NOTES

1. Cao, Q.; Rogers, J. A. Ultrathin Films of Single-Walled Carbon Nanotubes for Electronics and Sensors: A Review of Fundamental and Applied Aspects. *Adv Mater.* **2009**, *21*, 29–53.
2. Xiao, L.; Chen, Z.; Feng, C.; Liu, L.; Bai, Z.-Q.; Wang, Y.; Qian, L.; Zhang, Y.; Li, Q.; Jiang, K.; et al. Flexible, Stretchable, Transparent Carbon Nanotube Thin Film Loudspeakers. *Nano Lett.* **2008**, *8*, 4539–4545.
3. Wu, Q.; Zhang, C.; Liang, R.; Wang, B. Fire retardancy of a buckypaper membrane. *Carbon* **2008**, *46*, 1159–1174.
4. Wang, Z.; Liang, Z.; Wang, B.; Zhang, C.; Kramer, L. Processing and Property Investigation of Single-Walled Carbon Nanotube (SWNT) Buckypaper/Epoxy Resin Matrix Nanocomposites. *Composites, Part A* **2004**, *35*, 1225–1232.
5. Wang, S.; Liang, Z.; Pham, G.; Park, Y.-B.; Wang, B.; Zhang, C.; Kramer, L.; Funchess, P. Controlled Nanostructure and High Loading of Single-Walled Carbon Nanotubes Reinforced Polycarbonate Composite. *Nanotechnology* **2007**, *18*, 095708.
6. Thess, A.; Lee, R.; Nikolaev, P.; Dai, H.; Petit, P.; Robert, J.;

Xu, C.; Lee, Y. H.; Kim, S. G.; Rinzler, A. G.; et al. Crystalline Ropes of Metallic Carbon Nanotubes. *Science* **1996**, *273*, 483–487.
7. Rinzler, A. G.; Liu, J.; Dai, H.; Nikolaev, P.; Huffman, C. B.; Rodríguez-Macías, F. J.; Boul, P. J.; Lu, A. H.; Heymann, D.; Colbert, D. T.; et al. Large-Scale Purification of Single-Wall Carbon Nanotubes: Process, Product, and Characterization. *Appl. Phys. A: Mater. Sci. Process.* **1998**, *67*, 29–37.
8. Hennrich, F.; Lebedkin, S.; Malik, S.; Tracy, J.; Barczewski, M.; Rösner, H.; Kappes, M. Preparation, Characterization and Applications of Free-Standing Single Walled Carbon Nanotube Thin Films. *Phys. Chem. Chem. Phys.* **2002**, *4*, 2273–2277.
9. Sreekumar, T. V.; Liu, T.; Kumar, S.; Ericson, L. M.; Hauge, R. H.; Smalley, R. E. Single-Wall Carbon Nanotube Films. *Chem. Mater.* **2003**, *15*, 175–178.
10. Berhan, L.; Yi, Y. B.; Sastry, A. M.; Munoz, E.; Selvidge, M.; Baughman, R. Mechanical Properties of Nanotube Sheets: Alteration in Joint Morphology and Achievable Moduli in Manufacturable Material. *J. Appl. Phys.* **2004**, *95*, 4335–4345.
11. Wang, S.; Liang, Z.; Wang, B.; Zhang, C. High-Strength and Multifunctional Macroscopic Fabric of Single-Walled Carbon Nanotubes. *Adv. Mater.* **2007**, *19*, 1257–1261.
12. Malik, S.; Rösner, H.; Hennrich, F.; Böttcher, A.; Kappes, M. M.; Beck, T.; Auhorn, M. Failure Mechanism of Free Standing Single-Walled Carbon Nanotube Thin Films under Tensile Load. *Phys. Chem. Chem. Phys.* **2004**, *6*, 3540–3544.
13. Åström, J. A.; Krasheninnikov, A. V.; Nordlund, K. Carbon Nanotube Mats and Fibers with Irradiation-Improved Mechanical Characteristics: A Theoretical Model. *Phys. Rev. Lett.* **2004**, *93*, 215503.
14. Berhan, L.; Yi, Y. B.; Sastry, A. M. Effect of Nanorope Waviness on the Effective Moduli of Nanotube Sheets. *J. Appl. Phys.* **2004**, *95*, 5027–5034.
15. Girifalco, L. A.; Hodak, M.; Lee, R. S. Carbon Nanotubes, Buckyballs, Ropes, and a Universal Graphitic Potential. *Phys. Rev. B: Condens. Matter Mater. Phys.* **2000**, *62*, 13104–13110.
16. Arroyo, M.; Arias, I. Rippling and a Phase-Transforming Mesoscopic Model for Multiwalled Carbon Nanotubes. *J. Mech. Phys. Solids* **2008**, *56*, 1224–1244.
17. Buehler, M. J. Mesoscale Modeling of Mechanics of Carbon Nanotubes: Self-Assembly, Self-Folding, and Fracture. *J. Mater. Res.* **2006**, *21*, 2855–2869.
18. Cranford, S.; Yao, H.; Ortiz, C.; Buehler, M. J. A Single Degree of Freedom 'Lollipop' Model for Carbon Nanotube Bundle Formation. *J. Mech. Phys. Solids* **2010**, *58*, 409–427.
19. Zhigilei, L. V.; Wei, C.; Srivastava, D. Mesoscopic Model for Dynamic Simulations of Carbon Nanotubes. *Phys. Rev. B: Condens. Matter Mater. Phys.* **2005**, *71*, 165417.
20. Volkov, A. N.; Zhigilei, L. V. Mesoscopic Interaction Potential for Carbon Nanotubes of Arbitrary Length and Orientation. *J. Phys. Chem. C* **2010**, *114*, 5513–5531.
21. Volkov, A. N.; Simov, K. R.; Zhigilei, L. V. Mesoscopic Model for Simulation of CNT-Based Materials. Proceedings of the ASME International Mechanical Engineering Congress and Exposition, Boston, MA, October 31−November 6, 2008; ASME: New York, NY, IMECE2008-68021, 2008.
22. Volkov, A. N.; Zhigilei, L. V. Scaling Laws and Mesoscopic Modeling of Thermal Conductivity in Carbon Nanotube Materials. *Phys. Rev. Lett.* **2010**, *104*, 215902.
23. Volkov, A. N.; Simov, K. R.; Zhigilei, L. V. Mesoscopic Simulation of Self-Assembly of Carbon Nanotubes into a Network of Bundles. Proceedings of the 47th AIAA Aerospace Sciences Meeting, Orlando, FL, January 5−8, 2009; AIAA: Reston, VA, 2009−1544, 2009.
24. Wang, H.; Ghosh, K.; Li, Z.; Maruyama, T.; Inoue, S.; Ando, Y. Direct Growth of Single-Walled Carbon Nanotube Films and Their Optoelectric Properties. *J. Phys. Chem. C* **2009**, *113*, 12079–12084.
25. Cranford, S. W.; Buehler, M. J. In Silico Assembly and Nanomechanical Characterization of Carbon Nanotube Buckypaper. *Nanotechnology* **2010**, *21*, 265706.
26. Lee, S. W.; Kim, B.-S.; Chen, S.; Shao-Horn, Y.; Hammond, P. T. Layer-by-Layer Assembly of All Carbon Nanotube Ultrathin Films for Electrochemical Applications. *J. Am. Chem. Soc.* **2009**, *131*, 671–679.
27. Berendsen, H. J. C.; Postma, J. P. M.; van Gunsteren, W. F.; DiNola, A.; Haak, J. R. Molecular Dynamics with Coupling to an External Bath. *J. Chem. Phys.* **1984**, *81*, 3684–3690.
28. Abrams, Z. R.; Lereah, Y.; Hanein, Y. Transmission Electron Microscope Imaging of Single-Walled Carbon Nanotube Interactions and Mechanics on Nitride Grids. *Nanotechnology* **2006**, *17*, 4706–4712.
29. Chen, B.; Gao, M.; Zuo, J. M.; Qu, S.; Liu, B.; Huang, Y. Binding Energy of Parallel Carbon Nanotubes. *Appl. Phys. Lett.* **2003**, *83*, 3570–3571.
30. Abrams, Z. R.; Hanein, Y. Tube-Tube and Tube-Surface Interactions in Straight Suspended Carbon Nanotube Structures. *J. Phys. Chem. B* **2006**, *110*, 21419–21423.
31. Kis, A.; Csányi, G.; Salvetat, J.-P.; Lee, T.-N.; Couteau, E.; Kulik, A. J.; Benoit, W.; Brugger, J.; Forro, L. Reinforcement of Single-Walled Carbon Nanotube Bundles by Intertube Bridging. *Nat. Mater.* **2004**, *3*, 153–157.
32. Bhushan, B. Nanotribology of Carbon Nanotubes. *J. Phys.: Condens. Matter* **2008**, *20*, 365214.
33. Suekane, O.; Nagataki, A.; Mori, H.; Nakayama, Y. Static Friction Force of Carbon Nanotube Surfaces. *Appl. Phys. Express* **2008**, *1*, 064001.
34. Zhang, Y.; Iijima, S. Microscopic Structure of As-Grown Single-Wall Carbon Nanotubes by Laser Ablation. *Philos. Mag. Lett.* **1998**, *78*, 139–144.
35. Brenner, D. W. Empirical Potential for Hydrocarbons for Use in Simulating the Chemical Vapor Deposition of Diamond Films. *Phys. Rev. B: Condens. Matter Mater. Phys.* **1990**, *42*, 9458–9471.
36. Brenner, D. W.; Shenderova, O. A.; Harrison, J. A.; Stuart, S. J.; Ni, B.; Sinnott, S. B. A Second-Generation Reactive Empirical Bond Order (REBO) Potential Energy Expression for Hydrocarbons. *J. Phys.: Condens. Matter* **2002**, *14*, 783–802.
37. Zhang, Y. Y.; Tan, V. B. C.; Wang, C. M. Effect of Chirality on Buckling Behavior of Single-Walled Carbon Nanotubes. *J. Appl. Phys.* **2006**, *100*, 074304.
38. Stuart, S. J.; Tutein, A. B.; Harrison, J. A. A Reactive Potential for Hydrocarbons with Intermolecular Interactions. *J. Chem. Phys.* **2000**, *112*, 6472–6486.
39. Iijima, S.; Brabec, C.; Maiti, A.; Bernholc, J. Structural Flexibility of Carbon Nanotubes. *J. Chem. Phys.* **1996**, *104*, 2089–2092.
40. Yakobson, B. I.; Brabec, C. J.; Bernholc, J. Nanomechanics of Carbon Tubes: Instabilities Beyond Linear Response. *Phys. Rev. Lett.* **1996**, *76*, 2511–2514.
41. Kutana, A.; Giapis, K. P. Transient Deformation Regime in Bending of Single-Walled Carbon Nanotubes. *Phys. Rev. Lett.* **2006**, *97*, 245501.
42. Cao, G.; Chen, X. Buckling of Single-Walled Carbon Nanotubes upon Bending: Molecular Dynamics Simulations and Finite Element Method. *Phys. Rev. B: Condens. Matter Mater. Phys.* **2006**, *73*, 155435.
43. Zhu, J.; Pan, Z. Y.; Wang, Y. X.; Zhou, L.; Jiang, Q. The Effect of Encapsulating C_{60} Fullerenes on the bending Flexibility of Carbon Nanotubes. *Nanotechnology* **2007**, *18*, 275702.
44. Guo, X.; Leung, A. Y. T.; He, X. Q.; Jiang, H.; Huang, Y. Bending Buckling of Single-Walled Carbon Nanotubes by Atomic-Scale Finite Elements. *Composites, Part B* **2008**, *39*, 202–208.
45. Sun, Y.; Liew, K. M. The Buckling of Single-Walled Carbon Nanotubes upon Bending: The Higher Order Gradient Continuum and Mesh-Free Method. *Comput. Meth. Appl. Mech. Eng.* **2008**, *197*, 3001–3013.